The American Journal of Pathology, Vol. 177, No. 2, August 2010

DOI: 10.2353/ajpath.2010.091012

Cardiovascular, Pulmonary and Renal Pathology

Tubular Overexpression of Transforming Growth Factor-β1 Induces Autophagy and Fibrosis but Not Mesenchymal Transition of Renal Epithelial Cells

Robert Koesters,*† Brigitte Kaissling,‡ Michel LeHir,‡ Nicolas Picard,‡ Franziska Theilig,§ Rolf Gebhardt,¶ Adam B. Glick,‖ Brunhilde Hähnel,** Hiltraud Hosser,** Hermann-Josef Gröne,†† and Wilhelm Kriz**

From the Institute of Human Genetics, University of Heidelberg, Heidelberg, Germany; UMR_S 702, INSERM/University of Paris 6 (UPMC),† Hopital Tenon, Paris, France; the Institute of Anatomy,‡ University of Zurich, Zurich, Switzerland; the Institute of Vegetative Anatomy,§ Charité, University of Berlin, Berlin, Germany; the Institute of Biochemistry,¶ Medical Faculty, University of Leipzig, Leipzig, Germany; the Center for Molecular Toxicology and Carcinogenesis,‖ Department of Veterinary and Biomedical Sciences, The Pennsylvania State University, University Park, Pennsylvania; the Abteilung: Anatomie und Entwicklungsbiologie,** Medical Faculty Mannheim, University of Heidelberg, Mannheim, Germany; and the Division of Cellular and Molecular Pathology,†† German Cancer Research Center, Heidelberg, Germany*

We recently showed in a tetracycline-controlled transgenic mouse model that overexpression of transforming growth factor (TGF)-β1 in renal tubules induces widespread peritubular fibrosis and focal degeneration of nephrons. In the present study we have analyzed the mechanisms underlying these phenomena. The initial response to tubular cell-derived TGF-β1 consisted of a robust proliferation of peritubular cells and deposition of collagen. On sustained expression, nephrons degenerated in a focal pattern. This process started with tubular dedifferentiation and proceeded to total decomposition of tubular cells by autophagy. The final outcome was empty collapsed remnants of tubular basement membrane embedded into a dense collagenous fibrous tissue. The corresponding glomeruli survived as atubular remnants. Thus, TGF-β1 driven autophagy may represent a novel mechanism of tubular decomposition. The fibrosis seen in between intact tubules and in areas of tubular decomposition resulted from myofibroblasts that were derived from local fibroblasts. No evidence was found for a transition of tubular cells into myofibroblasts. Neither tracing of injured tubules in electron micrographs nor genetic tagging of tubular epithelial cells revealed cells transgressing the tubular basement membrane. In conclusion, overexpression of TGF-β1 in renal tubules *in vivo* induces interstitial proliferation, tubular autophagy, and fibrosis, but not epithelial-to-mesenchymal transition. ***(Am J Pathol 2010, 177:632–643; DOI: 10.2353/ajpath.2010.091012)***

The release of transforming growth factor (TGF)-β1 plays a central role in fibrosis following tissue injury. On the one hand, the formation of fibrous scars contributes to healing in various tissues. On the other hand, fibrosis is considered a driving force in the progression of chronic renal failure. Therefore, much effort has been made in unraveling the cellular and molecular processes, which underlie renal interstitial fibrosis. TGF-β1 is thought to trigger several mechanisms that lead to fibrosis, among them activation of resident fibroblasts and stimulation of tubular epithelial cells to transform into mesenchymal cells, ie, into fibroblasts and myofibroblasts.[1–5] This latter process is called epithelial-to-mesenchymal transition (EMT)[6,7]; its impact on fibrosis development in chronic renal disease is a matter of controversy.

We recently reported a tetracycline-inducible transgenic mouse model, in which conditional overexpression of TGF-β1 in renal tubules induced widespread peritubular fibrosis and focal nephron degeneration.[8] Thus, this model provides a unique tool to titrate parenchymal injury and fibrosis induced by TGF-β1. We used this model to study in detail the mechanism of tubular decomposition

Supported by Deutsche Forschungsgemeinschaft grants FOR406 (W.K. and R.K.), SFB 405 B10 (H.-J.G.), and by Prof. Dr. Karl und Gerhard Schiller-Stiftung (W.K.).

Accepted for publication April 21, 2010.

Address reprint requests to Prof. Dr. Wilhelm Kriz, Medizinische Fakultät Mannheim Universität Heidelberg, Abteilung: Anatomie und Entwicklungsbiologie, Ludolf-Krehl-Str. 13-17, Tridomus C, Ebene 6, D 68167 Mannheim. E-mail: wilhelm.kriz@urz.uni-heidelberg.de.

and the development of fibrosis in response to TGF-β1 including the role of EMT in these processes.

The damage induced by TGF-β1 overexpression was analyzed by structural and immunocytochemical techniques. In particular, we wanted to elucidate the sequence how tubules undergo decomposition and tubular cells participate in fibrosis development. An epithelial cell is a polarized cell with clearly separated apical and basolateral surfaces. A fibroblast/myofibroblast is an unpolarized cell generally with many cell processes. Thus, if an epithelial cell transforms into a fibroblastoid cell, we would expect to encounter intermediate stages with an intermediate transitional morphology. Moreover, renal tubular epithelial cells are strictly enclosed into a continuous cylinder of the tubular basement membrane (TBM). Thus, for a tubular cell to become a fibroblast/myofibroblast, it is not only necessary that it changes its morphology and its specific protein composition, but it has also to change its location. It has to leave the tubular compartment, to migrate through the TBM, and to take residency in the peritubular interstitium. Furthermore, it has to undergo a genetic reprogramming to (re)differentiate into a specialized different cell type. These changes in shape and in location should be detectable in usual histopathological specimens by high-resolution light and electron microscopy. In addition, we used fate-tracing techniques to identify the origin of cells involved in peritubular proliferation.

Materials and Methods

Animal Experiments

All experiments on live mice were approved by the governmental review committee on animal care at Regierungspräsidium Karlsruhe. Animal care and experimental procedures were conducted according to national standards and were permitted by local governmental authorities.

Housing

The mice were housed at a constant room temperature under standard nonsterile conditions, in groups of up to four animals. They were fed regular laboratory chow and water was supplied *ad libitum*. A 12-hour day and night cycle was maintained.

Transgenic Mice

Pax8-rtTA (genetic background: C57Bl6/DBA) is a transgenic line which expresses the reverse tetracycline-dependent transactivator (rtTA) under the control of a 4.3-kb fragment of the murine Pax8 promoter.[8]

Tet-o-TGF-β1 (genetic background: FVB/N) is a transgenic line in which the expression of the constitutively active Cys-Ser$^{223–225}$ double mutant form of porcine TGF-β1[9] is under control of the P_{tet} promoter.[10]

P_{tet}-TGF-β1 (genetic background: C57Bl6/DBA) is a similar, but independent transgenic line in which the expression of the constitutively active porcine TGF-β1 is under control of the bidirectional P_{tet} promoter.[11]

LC-1 (genetic background: C57Bl6/Balbc) is a transgenic line in which the expression of luciferase and cre recombinase is under control of the bidirectional P_{tet} promoter.[12]

Rosa26R (genetic background: 129/Sv) is a cre reporter line in which a cytosolic ß-galactosidase gene is under control of the ubiquitously active Rosa26 promoter. Expression is, however, conditional on the prior removal of a neo expression cassette which is flanked by loxP sites.[13]

For maintenance breeding, single transgenic mice were mated with C57Bl6 mice (Pax8-rtTA, LC1, P_{tet}-TGF-β1), FVB/N mice (tet-o-TGF-β1), or 129/Sv mice (Rosa26R).

Double transgenic PT mice were obtained from matings of single transgenic Pax8-rtTA and tet-o-TGF-β1 mice or P_{tet}-TGF-β1 mice. These mice were used for measuring TGF-β1 plasma levels. The genetic background of PT mice was mixed consisting of either C57Bl6/DBA/FVB/N (Pax8-rtTA/tet-o-TGF-β1) or C57Bl6/DBA (Pax8-rtTA/P_{tet}-TGF-β1).

For fate-tracing experiments, double transgenic PT (tet-o-TGF-β1) mice were mated with LC-1 mice to obtain triple transgenic PLT mice, and PLT mice were mated with Rosa26 mice to obtain quadruple transgenic PLRT mice. Since the efficiency of obtaining quadruple transgenic mice in this way is extremely low, PLRT mice were further expanded by inbreeding and used for cell fate tracing. The genetic background of PLRT mice was mixed consisting of C57Bl6/DBA/Balbc/129/Sv/FVB/N.

Genotyping

High molecular weight DNA was prepared from the tails of mice using QIAamp DNA mini kit (Qiagen, Hilden, Germany) and genotyping was performed by PCR. Pax8-rtTA primers were ST1: 5′-CCATGTCTAGACTGGACAAGA-3′, and ST2: 5′-CTCCAGGCCACATATGATTAG-3′. tet-o-TGF-β1 and P_{tet}-TGF-β1 primers were Tgfβ-fwd2: 5′-CCCAGTGACTCACCGGAGTGG-3′, and Tgfß-rev1: 5′-GTGTCTAGGCTCCAGATGTAGG-3′. LC-1 primers were Cre3: 5′-TCGCTGCATTACCGGTCGATGC-3′ and Cre4: 5′-CCATGAGTGAACGAACCTGGTCG-3′. Rosa26-R primers were Rosa26R-fwd1: 5′-AAAGTCGCTCTGAGTTTGTTAT-3′ and Rosa26R-rev1: 5′-GCGAAGAGTTTGTCCTCAACC-3′. The PCR conditions were set as follows: 1 cycle of 3 minutes 94°C, 35 cycles of (30s 94°C, 30s 52 to 60°C, and 30s 72°C), and 1 cycle of 7 minutes 72°C.

Experiments

Animals were exposed to doxycycline (Dox) at a concentration of 0.2 mg/ml dissolved in drinking water which contained 5% sucrose. Mice were sacrificed the day after the last Dox dose.

In total, we used 64 transgenic PT/PLRT responder mice treated with DOX for the different experimental groups. Fourteen transgenic PT/PLRT responder mice that were not treated with DOX and 14 nonresponder mice (either single-transgenic for P or T) that were treated with DOX, served as controls.

Thirty mice were continuously treated with DOX subdivided into subgroups: (a) treated for 2 days (9 mice) and (b) treated for 3 or 4 days (21 mice). Four (2 of a/2 of b) of these animals were perfused with glutaraldehyde to achieve optimal structural resolution. Six (0 of a/6 of b) of these animals were perfused with paraformaldehyde (PFA)/picric acid/cacodylate buffer and samples of these kidneys were shock-frozen to achieve optimal results by immunofluorescence. The remaining twenty mice (7 of a/13 of b) were perfused with PFA/PBS and used for all other techniques except immunofluorescence. This latter group included eight quadruple transgenic mice (PLRT), which served for fate tracing studies. Six single transgenic nonresponder mice treated with DOX and six responder mice left untreated served as controls.

Thirty-four mice were discontinuously treated with DOX subdivided in two subgroups: (a) treated up to five weekly cycles (13 mice) and (b) treated more than five weekly cycles (21 mice). Each cycle consisted of 2 days treatment with DOX and 5 days without treatment. Six (2 of a/4 of b) of these animals were perfused with glutaraldehyde, six (0 of a/6 of b) of these mice were perfused with PFA/picric acid/cacodylate buffer, and the remaining twenty-two mice (9 of a/13 of b) were perfused with paraformaldehyde/PBS. Again, the latter group included eight quadruple transgenic mice (PLRT) for fate tracing experiments. Eight single transgenic nonresponder mice treated with DOX and eight responder mice left untreated served as controls.

Determination of TGF-β1 by Enzyme-Linked Immunosorbent Assay

We collected blood samples into heparinized tubes by *retrobulbar* venous plexus punction. We centrifuged the samples for 5 minutes and took the supernatant plasma and assayed TGF-β1 protein levels by enzyme-linked immunosorbent assay without acid pretreatment with a commercially available kit (Promega #G7591, Mannheim, Germany).

Fixation

The animals were fixed by total body perfusion as described previously.[14] Briefly, under Narcoren anesthesia (10 mg per kg body weight, i.p.) or under ketamine-xylazine anesthesia (100 mg/6 mg per kg body weight, i.m.) the abdomen was opened and a cannula was retrogradely inserted into the abdominal aorta below the exit of the renal artery. Without prior flushing the animals were directly perfused with the fixative at a constant pressure of 100 mm Hg for 3 minutes. Three fixative solutions were used: (i) 2% glutaraldehyde phosphate buffer solution (GA-PBS) supplemented with 0.05% citric acid (pH 7.5; osmolarity, 485 mm osmol/L); (ii) 2% PFA pps (PFA-PBS; pH 7.4; osmolarity 900); and (iii) 3% PFA and 0.05% picric acid, dissolved in a 3:2 mixture of 0.1 mol/L cacodylate buffer (pH 7.4, adjusted to 300 mOsm with sucrose) and 10% hydroxyethyl starch in saline (Fresenius AG, Germany, PFA-Caco). The GA-PBS–perfused material was preferentially used for the structural, the PFA-PBS perfused material for the immunocytochemical studies and the PFA-Caco perfused tissue was used for immunofluorescence.

The kidneys were removed and cut into coronal slices, comprising the cortex and the outer medulla; they were frozen in liquid propane cooled with liquid nitrogen. From these slices, 2- to 3-μm thick sections were cut in a cryostat (Microm, Walldorf, Germany).

Sections were studied by epifluorescence with a Polyvar microscope (Reichert Jung, Vienna, Austria), and digital images were acquired with a CCD camera. Some slices of the PFA-Caco-fixed tissue were also embedded in paraffin to be used for the avidin-biotin technique (see below). The remaining tissue was used for structural studies (see below).

Structural Studies

Slices from kidney of all animals were postfixed in 2% GA-PBS overnight. Thereafter they were washed and cut into small blocks of cortex, which were postfixed in OSO4 (1% for 2 hours) and subsequently dehydrated and embedded into epon by standard procedures. Semithin (1 μm thick) sections from several blocks of each animal and, in addition, series of semithin sections (300 sections of selected blocks from animals of each group) as well as ultrathin sections of selected areas were cut on an ultracut microtome (Leica Nußloch Germany) using a diamond knife. Semithin sections were stained according to Richardson et al[15]) and examined with light microscopy; ultrathin sections were stained with uranyl acetate and lead citrate and studied with transmission electron microscopy (TEM).

Structural Evaluation—Tubular Tracings

We randomly selected low power transmission electron micrographs (×500 to ×1100) of tubular profiles of controls and transgenic mice at various stages of decomposition. Pictures of tubular profiles were taken from successive quadrangles of grid-mounted sections in a prefixed sequence. At least thirty profiles from each of six mice were taken. Since this proceeding yielded only few severely damaged tubules, we continued the sequence but considered only severely injured tubules (in total 42). Additional pictures were taken from two control mice.

We measured the tubular circumference along the TBM. We counted the cells (by counting the cell nuclei) inside the TBM and outside the TBM in the immediate surroundings, ie, in a belt of the thickness of half the tubular diameter (exclusive endothelial cells). We carefully traced the TBM surrounding each tubular profile for cells extending across the TBM.

Immunohistochemistry

PFA-perfused tissue was embedded in paraffin and 4-μm sections were cut. To optimize detection, the sections were microwaved five times for five minutes at 600 W in 0.01 mol/L sodium citrate buffer (pH 6.0) after dewaxing. Aldehydes were blocked with 0.1 mol/L ammonium chloride, nonspecific bindings of avidin and biotin were blocked with

the avidin/biotin blocking Kit (Vector-Alexis, Grünberg, Germany), and endogenous peroxidase was blocked with 3% H_2O_2. Afterward, the sections were stained with a ready-to-use Vectastain Elite ABC Kit Peroxidase (Vector-Alexis, Grünberg). As substrate-chromogen we used diaminobenzidine (DAB kit, Vector-Alexis, Grünberg).

The following antibodies (AB) were used: (i) polyclonal rabbit anti-rat type I collagen AB, reactive to mouse (1:100, Biotrend, Cologne, Germany); (ii) polyclonal rabbit anti-human α smooth muscle actin AB (α-SMA, reactive to mouse; 1:100; Abcam, Cambridge, UK); (iii) Ki-67 monoclonal rat anti-mouse AB (1:25), Fa, Dako Cytomation M7249, Clone TEC-3; (iv) polyclonal rabbit antibody, raised against human LC3B (N- terminal), reactive to human, mouse and rat LC3; Novus Biologicals, NB600-1384; (v) TGF-β1 polyclonal rabbit anti-human AB (1:100), Promega G1221; and (vi) FSP1/S100A4 polyclonal rabbit antibody raised against human S100A4 AB, reactive, among others, to rat and mouse, (1:1200), Dako Cytomation, Code A5114. For all antibodies, negative controls were used in which the primary antibody was omitted. All sections were negative.

Immunofluorescence Microscopy

Indirect immunofluorescence staining was performed with cryosections (2 to 3 μm) of the PFA-Caco perfused material; the following antibodies were used: (i) polyclonal rabbit anti Ecto-5 nucleotidase (5'NT) AB[16]; (ii) α-SMA: see above; (iii) MHC II monoclonal rat anti-mouse AB, FA, Clone OX 6; (iv) FSP1/S100A4: see above; and (v) ER-HR3 monoclonal rat anti-mouse AB, Acris, Bad Nauheim, Germany, Code BM4016.[17] For all antibodies, negative controls were used in which the primary antibody was omitted. All sections were negative.

Terminal Deoxynucleotidyl Transferase-Mediated dUTP Nick-End Labeling Assay

For detection of apoptotic cells we carried out a terminal deoxynucleotidyl transferase-mediated dUTP nick-end labeling assay (TUNEL; *In Situ* Cell Death Detection Kit, Roche, Basel) which uses peroxidase as a reporter. Four-μm paraffin sections of PFA-fixed material were dewaxed and rehydrated by standard methods. Endogenous peroxidase activity was inactivated and cells were permeabilized by short treatment with proteinase K. TUNEL reaction mixture was added and incubated at 37°C for 60 minutes. Detection was performed using diaminobenzidine as a substrate. Slides were counterstained with hematoxylin and mounted.

β-Galactosidase Assay

To reveal ß-galactosidase activity, samples were frozen in isopentane cooled in liquid nitrogen immediately after perfusion and stored at −80°C. We incubated 5 μm cryosections overnight in the dark in 5-bromo-4-chloro-3-indolyl βb-D-galactopyranoside (X-gal) solution (50 mmol/L Tris-HCl pH 7.5, 2.5 mmol/L potassium ferriferrocyanide, 15 mmol/L NaCl, 1 mmol/L $MgCl_2$, and 0.5 mg ml^{-1} X-gal) at 37°C. We counterstained cryosections with eosin and mounted them in Vitro-Clud (Fa. Langenbrinck, Emmendingen, Germany). Alternatively PFA-fixed tissue cubes were washed briefly in PBS and incubated in the above described X-gal staining solution at 37°C overnight with gentle agitation until the tissue was macroscopically intensely stained. Tissue cubes were washed in PBS, dehydrated in ethanol, and embedded in paraffin. Five-μm thick sections were slightly counterstained with eosin or were incubated with antibodies against collagen type I.

In Situ *Hybridization*

The mRNA expression of TGF-β1 was investigated by *in situ* hybridization using digoxigenin-labeled riboprobes (Roche). Sense and antisense probes were generated by *in vitro* transcription of a 500-bp porcine TGF-β1 cDNA template. *In situ* hybridization was performed on paraffin sections according to an established protocol.[18] Signal was generated with 4-nitroblue tetrazolium chloride.

We tested TGF-β1 sense and antisense probes in control and transgenic TGF-β1 overexpressing mice. Only TGF-β1 antisense probes in transgenic mice revealed specific staining in the typical mosaic expression pattern observed with the PAX8 promoter; the controls demonstrated no specific signal.

Quantifications and Statistics

Results are reported as mean ± SD; differences between the experimental and control animals in each group were tested with the unpaired *t*-test using Sigma Stat.

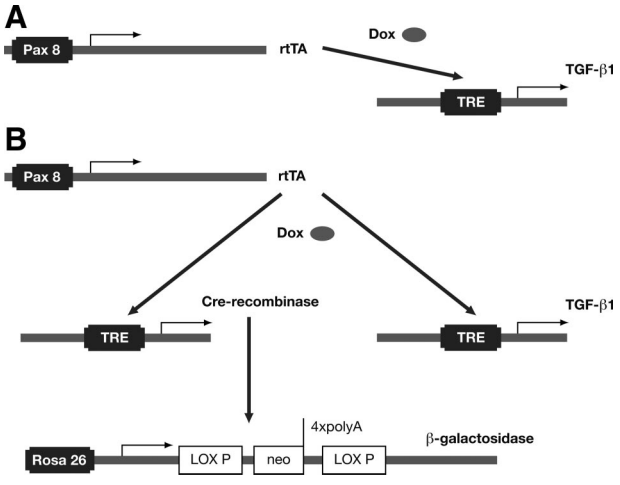

Figure 1. Experimental strategy. **A:** PT mice. We used PT (Pax8-rtTA/tet-o-TGF-β1 double transgenic) mice to direct TGF-β1 overexpression to renal epithelial cells. In these mice, rtTA is expressed under the control of the kidney-specific Pax8 promoter. rtTA binds to and transactivates the tetracycline-responsive element (TRE) but binding is dependent on the presence of doxycycline (DOX). Only when DOX is administered will TGF-β1 be expressed (Tet-on). **B:** PLRT mice. For fate-tracing experiments PLRT (Pax8-rtTA/LC1/Rosa26R/tet-o-TGF-β1 quadruple transgenic) mice were used. Pax8-rtTA directs the simultaneous expression of TGF-β1 and Cre recombinase. The latter enzyme removes the stop cassette at the Rosa26R locus, thereby irreversibly activating the expression of β-galactosidase from the Rosa26 promoter. Since the Rosa26 promoter is active in any cell type cells become genetically tagged.

Results

To analyze the role of TGF-β1 in renal fibrosis *in vivo*, we made use of a previously described transgenic mouse model of tetracycline-inducible overexpression of TGF-β1 in renal tubular epithelial cells.[8] In this model, TGF-β1 overexpression can be achieved in Pax8-rtTA/tet-o-TGF-β1 (PT) double transgenic mice by induction with doxycycline (DOX; Figure 1A and B). The Pax8 promoter targets the expression of TGF-β1 in a specific and highly efficient manner to renal tubular epithelial cells, whereas the integration of the tetracycline-inducible system at the same time allows tight temporal control of target gene expression. The latter is important to avoid embryonic lethality as well as acute toxicity associated with uncontrolled and sustained expression of TGF-β1.[11]

Tetracycline-responsive TGF-β1 transgenic mouse lines have been established by two different laboratories independently[10,11] and each line can be used in conjunction with Pax8-rtTA mice to model renal fibrosis. We initially compared both tetracycline-responsive TGF-β1 lines and found similar high plasma levels of TGF-β1 expression (>200 ng/ml; Figure 2, A–C) by enzyme-linked immunosorbent assay and similar acute toxicity on induction. Toxicity due to high systemic levels of TGF-β1 resulted in unsteady gait, shaggy fur, weight loss, and eventually death, when mice were treated with DOX for more than 4 days continuously. Similar general toxicity has been observed in a mouse model of liver-specific overexpression of TGF-β1.[11] To avoid early lethality, DOX

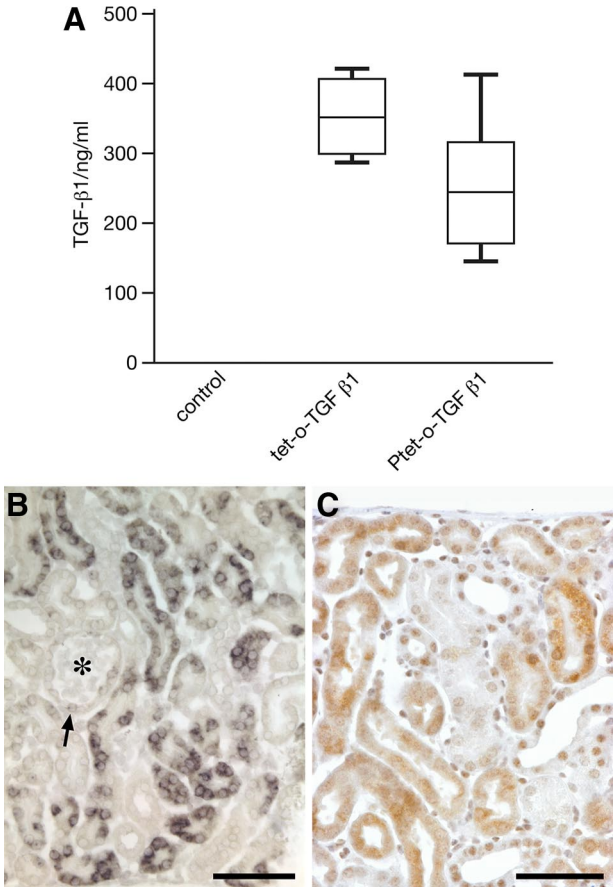

Figure 2. TGF-β1 expression. **A:** Plasma levels of TGF-β1 protein. Biologically active TGF-β1 protein in the plasma of induced mice (n = 6) was assayed by enzyme-linked immunosorbent assay. Control, Pax8-rtTA single transgenic mice induced for two days with doxycycline. Tet-o-TGF-β1, Pax8-rtTA/tet-o-TGF-β1 double transgenic mice induced for two days with doxycycline. Ptet-TGF-β1, Pax8-rtTA/Ptet-TGF-β1 double transgenic mice induced for two days with doxycycline. **B** and **C**: Tissue expression of TGF-β1 in Pax8-rtTA/tet-o-TGF-β1 double transgenic mice. **B:** *In situ* hybridization of TGF-β1 mRNA. Tubular cells are heterogeneously labeled; between no label and strong label all intermediates are found. The glomerular tuft (**asterisk**) is negative. The glomerular parietal epithelium in males frequently contains proximal tubule cells that are generally labeled (**arrow**; in this case only weakly). **C:** Immunostaining of TGF-β. At the protein level a heterogeneous pattern of TGF-β expression is also seen. PT mice, after three days (**B**), and after two days (**C**) of DOX stimulation. Scale bar = 50 μm.

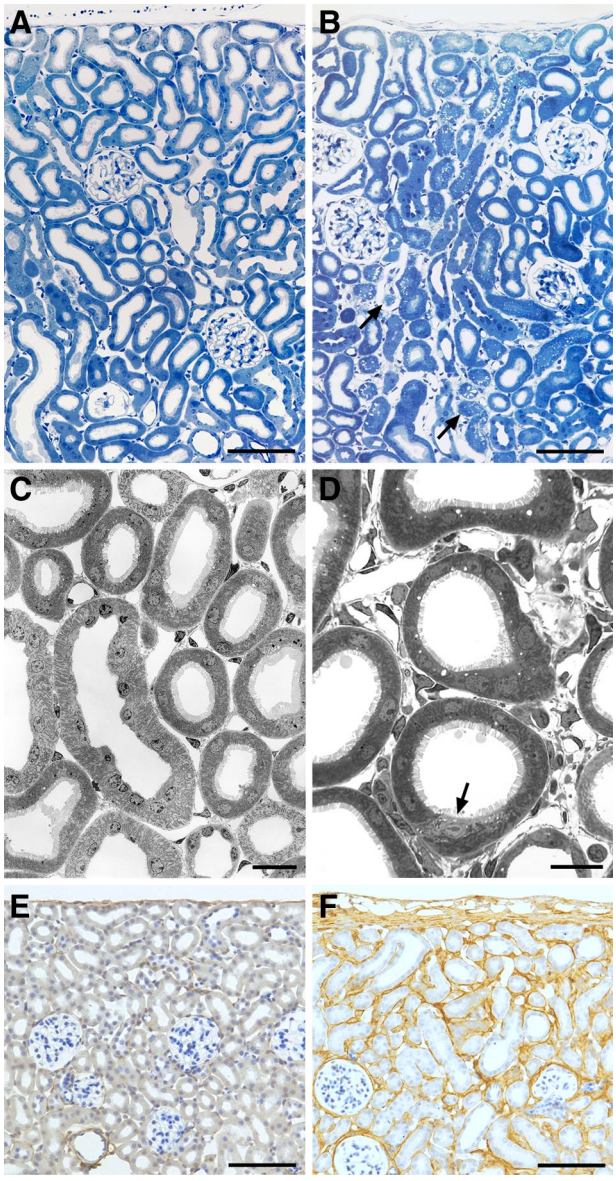

Figure 3. Early responses. **A** and **B**: Renal cortex, overview. Control (**A**); after four days of DOX (**B**), a massive expansion of the peritubular interstitium is seen; focally, tubules start to decompose (**arrows**). **C** and **D**: Cortical tubules and peritubular interstitium by TEM. Control (**C**); after 4 days (**D**) of DOX interstitial spaces and cells were dramatically increased; tubules are intact; focally, initial changes are seen (**arrow**). **E** and **F**: Renal cortex; immunostaining of collagen type 1 in controls (**E**) and after four days of stimulation (**F**). Note the diffuse deposition of collagen in (**F**); tubules maintain a normal structure. PT mice; Scale bars: 200 μm (**A**, **B**, **E**, **F**); 20 μm (**C**); and 10 μm (**D**).

was applied either continuously for 1 to 4 days or discontinuously in weekly cycles to get strong renal effects with tubular damage. In the latter mode mice were given DOX for only 2 days and then pure water for the remaining 5 days, for up to 10 cycles. Doxycycline alone did not have any adverse effect on renal histomorphology or function even after ten cycles of treatment in single transgenic (P or T) control mice.[8]

The tubular expression of the tet-o-TGF-β1 transgene basically comprised all tubular segments in the cortex and medulla, but was heterogeneous with respect to strength. After 2 to 4 days continuous treatment a majority of tubules, frequently arranged in groups, responded strongly at the mRNA and protein levels whereas others showed intermediate, weak, or barely detectable responses (Figure 2).

The earliest effects were seen in the peritubular interstitium already after 2 days of DOX stimulation and were very prominent after 4 days. They consisted of expansion and hypercellularity of the peritubular interstitium accompanied by a prominent increase in the content of collagen I (Figure 3, A–F); quantitatively, the increase in proliferating Ki-67 positive cells and the massive expansion of the peritubular space (by roughly 100% after 4 days) are shown in Table 1. Immunofluorescence revealed that the hypercellularity was due to a dramatic increase of 5′NT positive fibroblasts and the appearance of αSMA positive myofibroblasts (Figure 4, A–C); interstitial immunostaining for 5′NT and for αSMA was essentially congruent. Major histocompatibility class II-positive dendritic cells did not increase in number (data not shown). Mitotic figures in fibroblasts and myofibroblasts (Figure 4) confirmed the proliferation of these two cell types. Immunostaining for both was generally intimately apposed to the tubular basement membrane (Figure 4) generally of those tubules that showed initial signs of decomposition (shown below). The narrow apposition of capillaries to the outer circumference of tubules was generally lost; the capillaries were embedded midst in the interstitial tissue without any direct contact to tubules.

Table 1. Proliferation of Peritubular Cells and Interstitial Expansion

	Proliferating cells (Ki67positive)	Fractional interstitial volume, %
Controls (2 or 3 days DOX)	9.2 ± 3.98	13.2 ± 1.7
2 days DOX	33.2 ± 18.0**	21.8 ± 4.7*
3 or 4 days DOX	17.6 ± 13.4**	26.5 ± 3.2*
	(n = 5 per group)	(n = 6 per group)

Values are means ± SD; *P < 0.001 vs. control; **P < 0.02 vs. control.

Ki-67–positive cells in the peritubular space (comprising all cells encountered in between the tubules) dramatically increased after 2 days of DOX; after 3 or 4 days the number decreased compared to 2 days but was clearly significantly higher than in controls. DOX had no detectable effect on the cell proliferation; TGF-β1 negative transgenic animals stimulated with DOX and nonstimulated TGF-β1 positive transgenic animals did not show any difference; therefore the numbers were pooled.

The fraction of peritubular space (including the capillary space) dramatically increased in transgenic animals already after 2 days of DOX treatment and increased further after 3 or 4 days treatment.

S100A4 positive interstitial cells were not detected in controls; in experimental mice after 2 to 4 days of DOX stimulation few irregularly distributed positive cells were encountered in interstitial location (Figure 4); tubular cells never showed a positive signal.

Tubular changes were generally seen after 4 days of DOX treatment and became prominent in all animals with prolonged treatment (Figure 5, A–C). The tubular epithelia showed various structural aspects of lesions with focal areas of nephron decomposition and associated fibrosis (Figures 5, and 6, A–G). The lightest stages were focal tubular atrophy, wrinkling of the TBM, and accumulation of lysosomal elements in tubular cells. Proximal tubules in these stages showed distorted lumina due to local defects in the brush border and irregular basal outlines due to invagination and outpocketing of the TBM. The cells accumulated all kinds of lysosomal elements throughout the cell body (Figure 6). Mitochondria and the membranes of the basal labyrinth decreased.

In advanced stages the tubules were collapsed, remnant lumina were filled with cell debris. The cells increasingly separated from the TBM; they frequently became arranged in solid strands without any remnants of a tubular lumen (Figure 6). They contained huge multiform lysosomes, suggestive from appearance and composition to represent autophagosomes. The autophagic nature was confirmed by strong immunostaining for LC3 (Figure 6). The nuclei of such degenerating cells exhibited a normal chromatin pattern corroborated by the absence of positive TUNEL staining for apoptosis (Figure 6). Thus, the cells were decomposed by autophagy.

In even further advanced stages of tubular decomposition the heavily wrinkled cylinders of the TBM were empty or contained isolated cells filled with autophagic elements or just various amounts of cell debris (Figure 6). Until this stage of decomposition gaps in the TBM were not found. As revealed by tracing in serial sections the corresponding glomeruli were generally collapsed and had lost the connection to their former tubules.

The degenerating tubules and glomeruli were surrounded by a proliferating interstitial tissue that contained abundant type I collagenous matrix presenting as focal areas of severe fibrosis (Figure 5). The increased number of interstitial cells included fibroblasts, many myofibroblasts, a variable number of macrophages and only few S100A4 positive cells. Tubular positivity for S100A4 was never seen. ER-HR3-positive cells, considered as macrophages[17] were only inconsistently encountered (never in controls; data not shown).

Randomly selected (see *Materials and Methods*), 263 tubular profiles (83 profiles with no visible or slight damage but peritubular proliferation, 81 with intermediate stages of damage, 42 with severe stages of damage and 57 controls; Table 2) and their surrounding interstitium were inspected in electron micrographs with respect to cells transgressing the TBM. We counted the nuclei of the epithelial cells inside the TBM compartment and the nuclei of all peritubular cells (except those of endothelial cells) in the immediate vicinity (corresponding to a belt of about the thickness of half the tubular diameter). These assessments showed the progressive decrease in tubu-

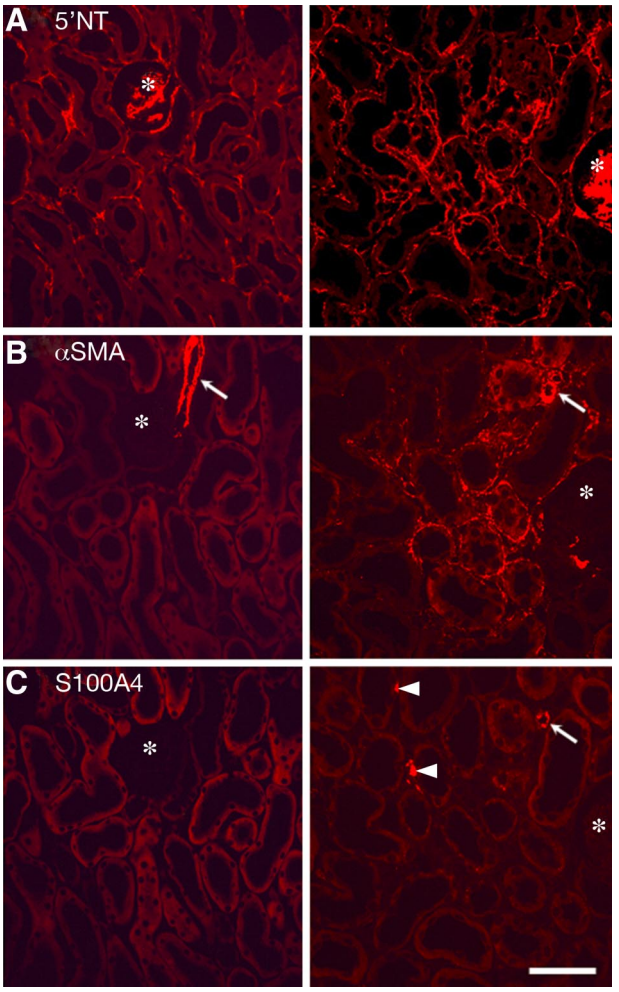

Figure 4. Immunocytochemistry. Immunostaining of peritubular cells for 5′NT (**A**), αSMA (**B**), and S 100A4 (**C**) in controls (**left column**) and PT mice (**right column**). The three pictures of each column are taken from consecutive sections, thus they show the same area; note the position of the glomerulus (**asterisk**). **A:** In addition to peritubular fibroblasts the brush border of proximal tubules and the mesangium (specifically in mice) stains with 5′NT; the interstitial 5′NT positive cells were much more abundant after TGF-β stimulation. **B:** αSMA-positive peritubular cells are not present in controls; only the smooth muscle cells of a glomerular arteriole are stained (**arrows**). After DOX treatment there is a dramatic appearance of αSMA-positive cells around affected tubules. The interstitial sites of 5′NT and αSMA positivity are congruent. **C:** No S100A4-positive cells are found in controls; a few cells are found after DOX treatment in interstitial position (**arrowheads**); they possibly represent lymphocytes. The smooth muscle cells of arterioles (**arrow**) are also stained. PT mice after three days of DOX. Scale bar = 20 μm.

lar cells and the increase in peritubular cells. We carefully looked at the 206 tubular profiles from experimental animals for gaps in the TBM and cells crossing the TBM. In the present model, splitting or doubling of the TBM was never seen permitting a clear-cut tracing of the TBM in every case. We did not find any cells crossing the TBM suggestive for cell migration from inside to outside or in the opposite direction. Furthermore, the tracings revealed that frequently the TBM of degenerating tubules was extremely wrinkled so that stronger powered transmission electron micrographs were necessary to trace the exact borders and to decide whether a cellular profile is located in- or outside the TBM (Figures 6, A–D; and 7, A–B). Collagen I was never found inside tubular remnants, even in cases of fully cell-depleted TBM-cylinders (Figures 6, C and D).

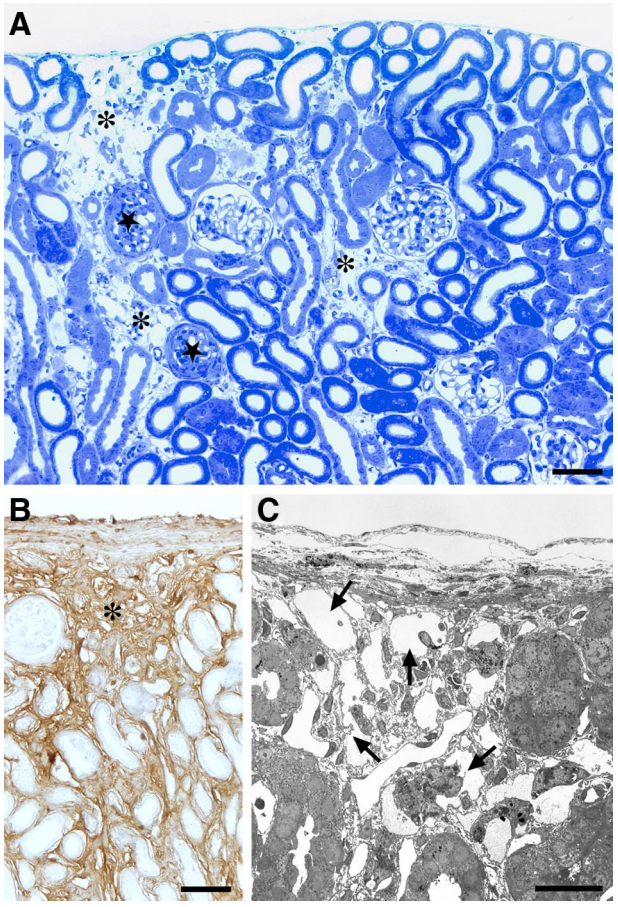

Figure 5. Tubular degeneration after prolonged treatment with DOX. **A:** Cortex, overview. Areas with tubular decomposition (**asterisks**) are intermingled with areas of normal tubules. A collapsed or sclerotic glomerulus (**stars**) is generally found adjacent to an area with tubular degeneration. **B:** Immunostaining of collagen I. Area of tubular decomposition (**asterisk**) that contains large amounts of collagen I. **C:** Overview of an area of tubular decomposition (TEM). The tubular remnants (**arrows**) consist of cylinders of TBM largely devoid of cells. PT mice: **A** and **C** after three, and **B** after six cycles of DOX. Scale bars: 100 μm (**A**) and (**B**); 20 μm (**C**).

To further study the role of TGF-β1 in the induction of EMT, we traced the fate of renal tubular cells by genetic tagging. By crossing we established quadruple transgenic mice of the genotype Pax8-rtTA/LC1/Rosa26R/tet-o-TGF-β1 (PLRT; Figure 1B). In PLRT mice administration of DOX triggers the simultaneous expression of TGF-β1 and cre recombinase in all Pax8-positive renal tubular epithelial cells. Cre recombinase expression causes recombination at the Rosa26R locus, which leads to activation of a cytosolic β-galactosidase reporter gene. Since recombination is irreversible, Pax8-positive cells become genetically tagged even when activation of the tetracycline-responsive element would occur only temporarily. Thus, using Cre-loxP recombination, the tubular cell lineage was genetically labeled with β-galactosidase in an irreversible manner (Figure 1B).

When treated with DOX, the kidneys of PLRT mice showed interstitial proliferation and matrix production, focal nephron degeneration and associated fibrosis, essentially the same phenotype as in the PT mice described

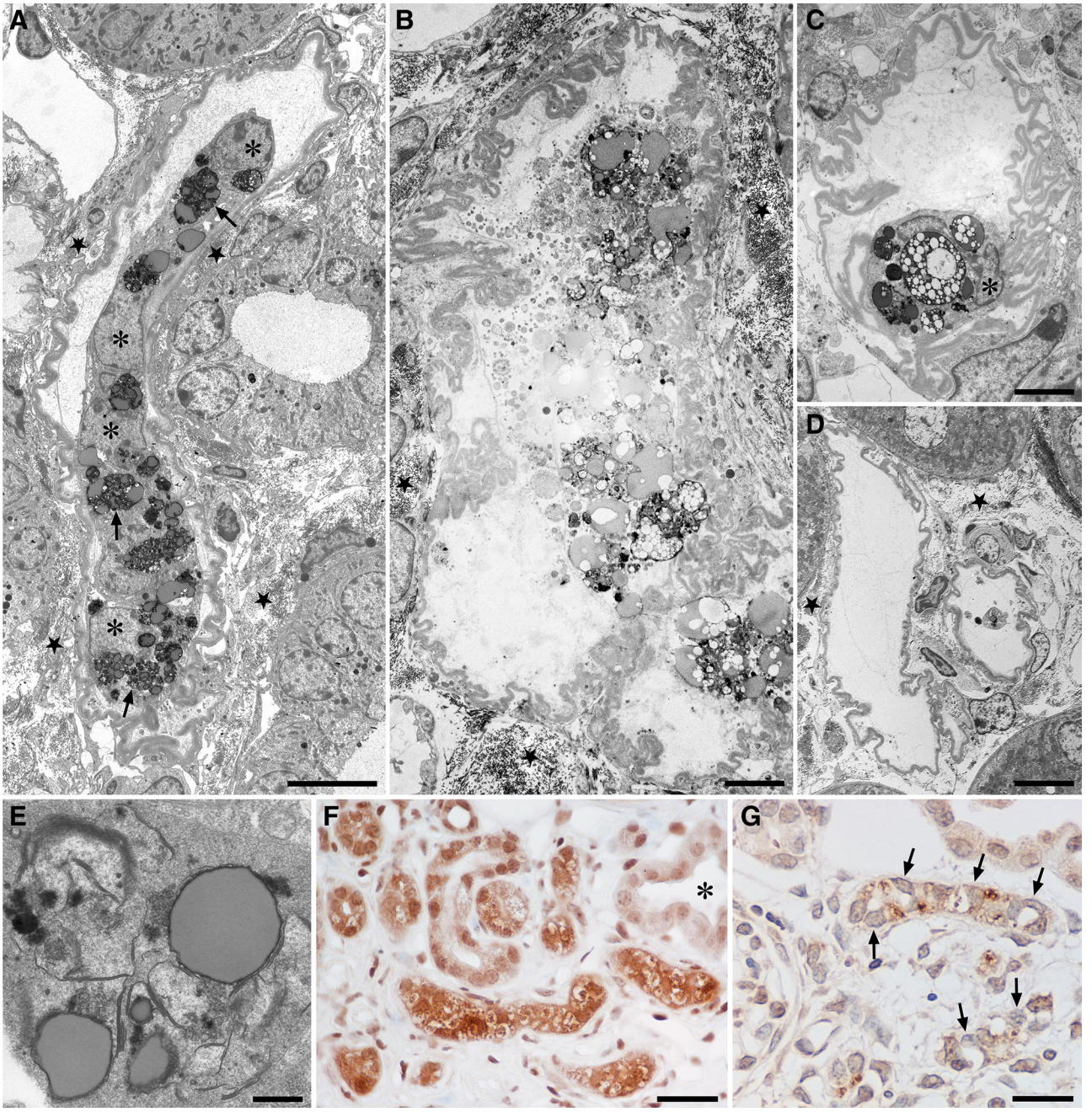

Figure 6. Decomposition of tubules by autophagy**. A:** Overview of a tubular profile at an intermediate stage of decomposition. The cells have separated from the TBM and joined to a single strand, the tubular lumen is fully lost. The cells contain large amounts of autophagic vacuoles (**arrows**). Note that the cell nuclei do not show apoptotic condensations (**asterisks**). The TBM is thickened and heavily wrinkled; gaps in the TBM are not seen. Outside the TBM collagen is accumulated (**star**). **B–D:** Late stages of tubular decomposition. **B:** A remnant tubular profile, bordered by a heavily wrinkled, but continuous TBM, containing the debris of several bursting cells; outside the TBM large amounts of collagen are seen (**star**). **C:** Tubular profile that contains a single cell with large autophagic vacuoles; the nucleus (**asterisk**) shows no signs of apoptosis. **D:** Empty wrinkled TBM profiles. Collagen is only encountered in the surroundings (**star**). **E:** Autophagic elements with many double membranes as are characteristic for autophagy. **F:** Degenerating tubular profiles are strongly stained for LC3; intact tubules (**asterisk**) are unstained. **G:** A group of degenerating tubules; the nuclei are unlabeled (**arrows**) in the TUNEL assay. PT mice: **A** to **D**, **F** and **G** six cycles, **E** three cycles of DOX. Scale bars: 10 μm (**A** and **D**), 4 μm (**B** and **C**), 1 μm (**E**), and 20 μm (**F** and **G**).

above. The expression of ß-galactosidase strictly correlated with collagen deposition, which we used as a substitute marker for TGF-β1 activity (Figure 8A). Degenerating tubular cells gradually lost the label, fading remnants were regularly encountered within otherwise empty TBM profiles (Figures 8, B–E). Even in areas with a high fraction of labeled tubular cells and labeled remnants (Figure 8C), we did not find expression of ß-galactosidase in the interstitium.

Discussion

Overexpression of TGF-β1 in renal tubules in the present model had two major consequences. First, it induced a mild to moderate diffuse fibrosis that was observed already at day 2 and preceded any tubular damage. Second, starting after 4 days of treatment it initiated tubular decomposition in a focal pattern with massive fibrosis.

Table 2. Analysis of Individual Tubular Profiles

	Total number of profiles studied (*N*)	Total tubular circumference studied (L;mm)	Cell nuclei inside the TBM Total number Divided by *N* Divided by L	Cell nuclei in the vicinity (except endothelial cells). Total number Divided by *N* Divided by L	Cells transgressing the TBM
Control mice	57	7.46	226 4.0 30.3	79 1.4 10.6	0
DOX treated transgenic mice					
with interstitial changes only	83	10.89	418 5.04 38.4	324 3.9 29.8	0
with tubular lesions of moderate severity	81	9.97	420 5.2 42.1	397 4.9 39.8	0
with severe tubular damage	42	6.0	85 2.0 14.2	210 5.0 35.0	0

Assessments were done in TEMs that generally showed 1 to 3 tubular profiles; in total 263 profiles (*N*) with a total circumference (L) of 34,3 mm were inspected. The cell nuclei inside the TBM and the cell nuclei of all peritubular cells (except those of endothelial cells) in the immediate vicinity (ie, located in a belt of the thickness of half the tubular diameter) were counted. Note, that the number of cell nuclei inside strongly decreased whereas the number of cell nuclei outside increased. No cells transgressing the tubular basement membrane were found.

The early effects consisted of peritubular proliferation and matrix accumulation but without tubular injury. An obvious mechanism of interstitial cell accumulation was the proliferation of resident fibroblasts as revealed by Ki-67 staining of 5′NT-positive cells and also by TEM (frequent mitotic figures in fibroblasts). The myofibroblasts that were encountered already on day 2 appeared to be derived, at least in part, also from resident fibroblasts as suggested by expression of αSMA by 5′NT positive cells. Later myofibroblasts themselves proliferated. Similar findings were recently reported in an unilateral ureteral obstruction model of renal fibrosis.[19]

Evidence for EMT as a contributor to the peritubular hypercellularity was not found at this early stage. The tubules were intact, tubular cells did not show any severe changes; careful tracing of tubular profiles by TEM did not reveal any gaps, defects in the TBM nor any cells crossing this barrier; S100A4 positivity was never seen in tubular cells neither at this early stage nor later. These results agree with a previous study in mice,[20] in which overexpression of TGF-β1 in the juxtaglomerular apparatus also produced peritubular fibrosis, but without tubular damage or any evidence for EMT.

The late stages of the disease were characterized by focal areas of nephron degeneration associated with dense local fibrosis. This raises two questions: (i) why and how did the nephrons undergo decomposition and (ii) is there a contribution of injury-driven EMT to the massive fibrosis surrounding and finally replacing the dying nephrons?

Nephron decomposition in this model generally started in the tubules; glomerular degeneration occurred secondarily to the tubular damage. Early lesions were seen at any site of a tubule including proximal tubular epithelia that extended into Bowman' capsule. It is likely that the tubular injury represented a direct toxic effect of sustained high doses of TGF-β1 in the cells in which it was produced. Accordingly, the focal pattern of tubular injury corresponded to the heterogeneous expression pattern of the transgenes as seen in the β-galactosidase pattern, by *in situ* hybridization and by immunochemistry against TGF-β1 (Figures 2 and 8). Thus, the focal pattern of tubular decomposition and fibrosis in the present model, though similar in appearance, is caused by a totally different mechanism than that starting from a primary glomerular disease as known from other models of acquired tubulo-interstitial diseases.[21–22]

The process of tubular decomposition started with tubular atrophy, followed by collapse and disconnection of the cells from the TBM. Finally, the cells died by autophagy. Signs of cell apoptosis were not encountered. Accumulation of lysosomal elements throughout the cell was the first sign of the autophagic process, as clearly seen in TEM (various cell organelles partially surrounded by doubled membranes) and confirmed by LC3 positivity (Figure 6F); the LC3 protein is stably associated with autophagosome membranes.[23,24] In the course of this process the remnants of one cell were obviously removed by phagocytosis by neighboring cells. Whether this mechanism includes fratricide of still intact cells as suggested for tubular atrophy[25] remains to be established. This finally led to almost cell-free cylinders of the TBM, which became increasingly wrinkled and eventually collapsed. The TBM maintained its continuity for considerable time after collapsing. The surprising finding was the complete local disappearance of any cellular elements inside these cylinders. Cells crossing the TBM border of these complex structures were not encountered, neither any macrophages entering, nor any tubular cells leaving. Outside these degenerating tubules/tubular remnants, a vivid cell proliferation (Figures 4 and 5; Table 1) was encountered associated with progressing deposition of extracellular matrix, predominantly collagen type I. Inside

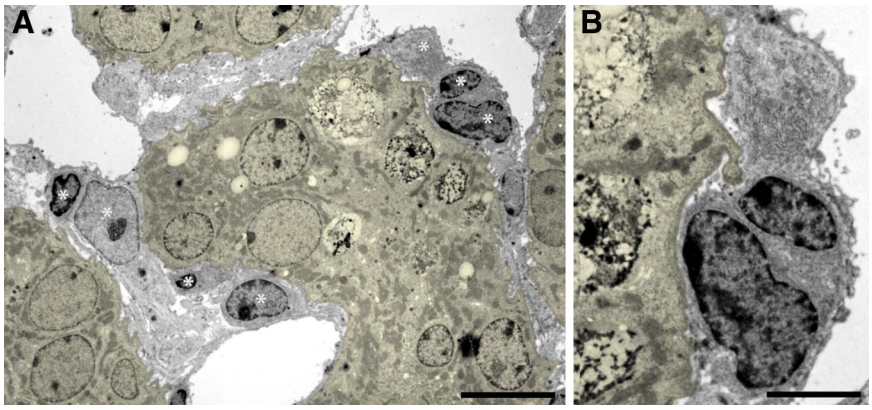

Figure 7. Outline of tubular basement membrane. To trace the exact borders of degenerating tubules low power transmission electron micrographs are frequently insufficient. In **A** several injured tubules are highlighted in yellow. Without this labeling it would be difficult to decide whether some cells (**asterisks**) are located inside or outside the tubular basement membrane. The higher magnified picture in **B** clearly allows a separation. PT mouse after 4 days DOX. Scale bars: 10 μm (**A**); 5 μm (**B**).

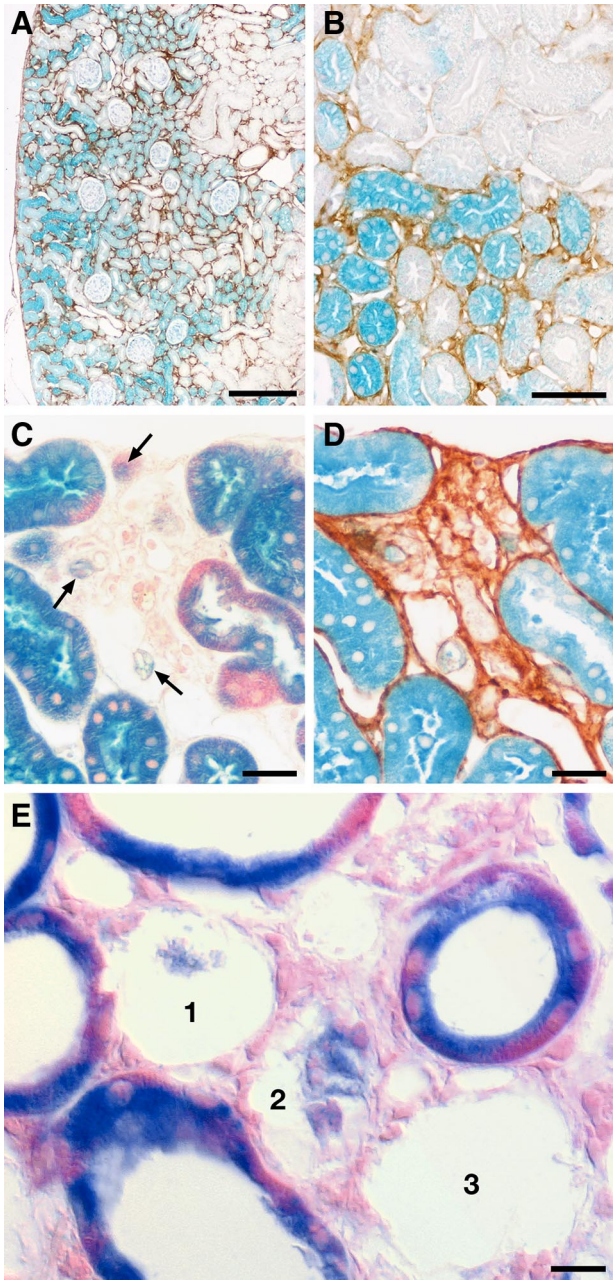

the TBM compartment collagen was never seen, apart from very late stages when the wrinkled remnants of the TBM gradually disappeared (probably by local digestion). Surprisingly, even in this stage of the disease macrophages were only rarely encountered.

As has become known in recent years, autophagy represents another mechanism of programmed cell death—in addition to apoptosis.[26–29] Ultrastructurally, cells dying along this pathway were characterized by the occurrence of multiple large autophagolysosomes (autophagic vacuoles), but without any nuclear or cytoplasmic condensations; thus the nuclei, in contrast to apoptosis, maintain a normal pattern in the beginning of this process.

Autophagic programmed cell death has so far not been considered as a mechanism for tubular cell death on its own. It has been discussed as a cytoprotective mechanism in tubular cells in response to exposure to potentially toxic substances, like cisplatin[30] and cyclosporine.[31] In this context autophagy has been interpreted as to counterbalance ER stress-induced ER expansion.[32,33]

In other organs autophagy has well been shown to cause cell death on its own.[29] In the present study the epithelial cell-substructure together with the tempestuous way of tubular degeneration suggested that sustained TGF-β1 induced cell death by autophagy. The abundance of autophagic vacuoles (LC3 positive) filling the cytoplasm of cells that have normal-appearing nuclei (TUNEL negative) clearly identifies autophagy as the mechanism leading to tubular cell death. The autophagocytic process culminates in epithelial cell lysis with rem-

Figure 8. Tracing for tubule derived cells after permanent labeling with LacZ. **A** and **B:** LacZ expression shown by β-galactosidase staining co-stained with antibodies to collagen I. Note that the heterogeneous expression of LacZ (indicative of TGF-β expression) perfectly correlates with peritubular collagen deposition (brown). No labeled cells are encountered in peritubular spaces. Overview (**A**) and detail from a consecutive section (**B**). **C** and **D** show the same area of tubular degeneration in two consecutive sections, in (**C**) co-stained with eosin, in (**D**) against collagen type I. The dense collagenous fibrosis of the area is clearly seen in (**D**). The tubular remnants within this area show a pale staining (**arrows** in C); no labeled interstitial cells are seen. **E:** Area of tubular degeneration and interstitial fibrosis. Cells of intact tubules are strongly labeled with β-galactosidase. Three profiles (**1**,**2**,**3**) of degenerating tubules are seen, two of them contain cellular remnants that show a fading staining. Cells in the interstitium are not labeled. PLRT mice (**A**) and (**B**) after 4 days, (**C**) and (**D**) after six cycles and (**E**) after three cycles of DOX. Scale bars: 200 μm (**A**), 50 μm (**B**), 20 μm (**C** and **D**), and 10 μm (**E**).

nants removed either by urine flow or through heterophagy by neighboring tubular cells.

The underlying mechanisms triggering the violent autophagy in response to TGF-β1 are unknown. An early and total disconnection of cells from the TBM was among the characteristic features of tubular degeneration in the present model. Epithelial cells critically depend on integrin-mediated cell adhesion to ECM for proper growth and survival. Detachment of epithelial cells from the matrix (anoikis) is known to trigger autophagy.[34] However, whether this is of any relevance under the present circumstances remains to be established.

Surprisingly, the present observations of tubular degeneration are similar in essential features to tubular decomposition secondary to a primary glomerular disease with obstruction of the glomerulo-tubular junction.[21,22,35] Though tubular decomposition subsequent to tubular obstruction generally proceeds more slowly, the individual stages are similar: shrinkage, atrophy, accumulation of abundant lysosomal elements, detachment from the TBM, and maintenance of a normal nuclear structure, finally ending up as empty wrinkled profiles of TBM. Thus, autophagy seems to play a major role under these settings, as well. One may speculate that the autophagic mechanism is a more appropriate kind of programmed cell death than apoptosis because macrophages do not have early access to the inner TBM-compartment during tubular degeneration. The autophagic type of programmed cell death as a cytokine driven mechanism has not been described before in tubules, but—possibly as a slower variant—may well underlie the decomposition of "aglomerular tubular remnants" as seen in "classical" chronic models of tubular degeneration.

With respect to injury triggered EMT we found no evidence that the process of TGF-β1 driven tubular autophagy included a branch to EMT. Despite the rapid and progressive depletion of tubular cells inside the cylinders of the TBM and the marked increase in peritubular myofibroblasts, no cells crossing the border of the TBM were encountered.

Also in our genetic fate tracing experiments we did not find β-galactosidase labeled cells in the extratubular compartment. Thus, we found no evidence of a participation of EMT to fibrosis in the present model.

The present study joins those that did not find evidence for a contribution of EMT to renal fibrosis. The pros[1–7] and cons[19,20,36–42] to this question are derived from a broad spectrum of different studies, *in vivo* versus *in vitro* studies as well as from different animal models. This raises the question whether EMT is dependent on specific circumstances. In the present transgenic *in vivo* model, fibrosis developed directly in response to TGF-β1, which is considered as the major cytokine to induce EMT.[1–5] Thus, even within this seemingly favorable context EMT was not observed.

In summary, it has been long appreciated that TGF-β1 is a pluripotent substance[43]; depending on dose it may have even opposing effects.[44,45] These findings uncover a novel potential role of TGF-β1, ie, the induction of autophagy in renal epithelial cells. Its relevance under more usual pathological conditions as a possible further mechanism of programmed cell death remains to be established.

Acknowledgments

We thank Philippe Soriano (Fred Hutchinson Cancer Research Center) for providing Rosa26R mice, Irina Voehringer, and Jeanette Charon-Alvarez for technical assistance; the teams of the animal facilities at Deutsches Krebsforschungszentrum and Interfakultäre Biomedizinische Forschungseinrichtung Heidelberg for animal caretaking; Tjeerd Sijmonsma for skillful and expert handling of the mice; Shijun Wang for help with tissue preservation and Rolf Nonnenmacher for graphical work.

References

1. Miettinen P, Ebner R, Lopez A, Derynck R: TGF-beta induced transdifferentiation of mammary epithelial cells to mesenchymal cells: involvement of type I receptors. J Cell Biol 1994, 127:2021–2036
2. Fan J, Ng Y, Hill P, Nikolic-Paterson D, Mu W, Atkins R, Lan H: Transforming growth factor-beta regulates tubular epithelial myofibroblast transdifferentiation in vitro. Kidney Int 1999, 56:1455–1467
3. Zavadil J, Bitzer M, Liang D, Yang Y, Massimi A, Kneitz S, Piek E, Bottinger E: Genetic programs of epithelial cell plasticity directed by transforming growth factor-beta. Proc Natl Acad Sci USA 2001, 98:6686–6691
4. Gotzmann J, Mikula M, Eger A, Schulte-Hermann R, Foisner R, Beug H, Mikulits W: Molecular aspects of epithelial cell plasticity: implications for local tumor invasion and metastasis. Mutat Res 2004, 566:9–20
5. Zeisberg E, Kalluri R: The role of epithelial-to-mesenchymal transition in renal fibrosis. J Mol Med 2004, 82:175–181
6. Zeisberg E, Tarnavski O, Zeisberg M, Dorfman A, McMullen J, Gustafsson E, Chandraker A, Yuan X, Pu W, Roberts A, Neilson E, Sayegh M, Izumo S, Kalluri R: Endothelial-to-mesenchymal transition contributes to cardiac fibrosis. Nat Med 2007, 13:952–961
7. Kalluri R, Neilson E: Epithelial-mesenchymal transition and its implications for fibrosis. J Clin Invest 2003, 112:1776–1784
8. Traykova-Brauch M, Schönig K, Greiner O, Miloud T, Jauch A, Bode M, Felsher D, Glick A, Kwiatowski D, Bujard H, Horst J, von Kebel Doeberitz M, Niggli F, Kriz W, Gröne H, Koesters R: An efficient and versatile system for acute and chronic modulation of renal tubular function in transgenic mice. Nat Med 2008, 14:979–984
9. Samuel S, Hurta R, Kondaiah P, Khalil N, Turley E, Wright J, Greenberg A: Autocrine induction of tumor protease production and invasion by a metallothionein-regulated TGF-beta 1 (Ser223,225). EMBO J 1992, 11:1599–1605
10. Liu X, Alexander V, Vijayachandra K, Bhogte E, Diamond I, Glick A: Conditional epidermal expression of TGFbeta 1 blocks neonatal lethality but causes a reversible hyperplasia and alopecia. Proc Natl Acad Sci USA 2001, 98:9139–9144
11. Ueberham E, Löw R, Ueberham U, Schonig K, Bujard H, Gebhardt R: Conditional tetracycline-regulated expression of TGF-β1 in liver of transgenic mice leads to reversible intermediary fibrosis. Hepatology 2003, 37:1067–1078
12. Schonig K, Schwenk F, Rajewsky K, Bujard H: Stringent doxycycline dependent control of CRE recombinase in vivo. Nucleic Acids Res 2002, 30:e134
13. Soriano P: Generalized lacZ expression with the ROSA26 Cre reporter strain. Nat Genet 1999, 21:70–71
14. Kaissling B, Kriz W: Variability of intercellular spaces between macula densa cells: A transmission electron microscopic study in rabbits and rats. Kidney Int 1982, 22(Suppl 12):9–17
15. Richardson K, Jarett L, Finke E: Embedding in epoxy resins for ultrathin sectioning in electron microscopy. Stain Technol 1960, 35:313–325
16. Dawson T, Gandhi R, Le Hir M, Kaissling B: Ecto-5′-nucleotidase:

localization in rat kidney by light microscopic histochemical methods. J Histochem Cytochem 1989, 37:39–47
17. de Jong J, Leenen P, Voerman J, van der Sluijs-Gelling A, Ploemacher R: A monoclonal antibody (ER-HR3) against murine macrophages. II. Biochemical and functional aspects of the ER-HR3 antigen. Cell Tissue Res 1994, 275:577–585
18. Theilig F, Bostanjoglo M, Pavenstadt H, Grupp C, Holland G, Slosarek I, Gressner A, Russwurm M, Koesling D, Bachmann S: Cellular distribution and function of soluble guanylyl cyclase in rat kidney and liver. J Am Soc Nephrol 2001, 12:2209–2220
19. Picard N, Baum O, Vogetseder A, Kaissling B, Le Hir M: Origin of renal myofibroblasts in the model of unilateral ureter obstruction in the rat. Histochem Cell Biol 2008, 130:141–155
20. Chai Q, Krag S, Chai S, Ledet T, Wogensen L: Localisation and phenotypical characterisation of collagen-producing cells in TGF-β1-induced renal interstitial fibrosis. Histochem Cell Biol 2003, 119:267–280
21. Kriz W, Hosser H, Haehnel B, Gretz N, Provoost A: From segmental glomerulosclerosis to total nephron degeneration and interstitial fibrosis: a histopathological study in rat models and human glomerulopathies. Nephrol Dial Transplant 1998, 13:2781–2798
22. Kriz W, Haehnel B, Hosser H, Ostendorf T, Kränzlin B, Gretz N, Shimizu F, Floege J: Pathways to recovery and loss of nephrons in anti-Thy-1 nephritis. J Am Soc Nephrol 2003, 14:1904–1926
23. Kabeya Y, Mizushima N, Yamamoto A, Oshitani-Okamoto S, Oshumi Y, Yoshimori T: LC3, GABARAP, and GATE16 localize to autophagosomal membrane depending on form-II formation. J Cell Sci 2004, 117:2805–2812
24. Mizushima N: Methods for monitoring autophagy. IJBCB 2004, 36:2491–2502
25. Schelling J, Cleveland R: Involvement of Fas-dependent apoptosis in renal tubular epithelial cell deletion in chronic renal failure. Kidney Int 1999, 56:1313–1316
26. Bursch W, Ellinger A, Gerner C, Fröhwein U, Schulte-Hermann R: Programmed cell death (PCD): apoptosis, autophagic PCD, or others? Ann NY Acad Sci 2000, 926:1–12
27. Cuervo A: Autophagy: many paths to the same end. Mol Biol Cell 2004, 263:55–72
28. Kundu M, Thompson C: Autophagy: basic principles and relevance to disease. Annu Rev Pathol 2008, 3:427–455
29. Scarlatti F, Granata R, Meijer A, Codogno P: Does autophagy have a license to kill mammalian cells? Cell Death Differ 2009, 16:12–20
30. Periyasamy-Thandavan S, Jiang M, Wei Q, Smith R, Yin X, Dong Z: Autophagy is cytoprotective during cisplatin injury of renal proximal tubule cells. Kidney Int 2008, 74:631–640
31. Pallet N, Bouvier N, Legendre C, Gilleron J, Codogno P, Beaune P, Thervet E, Anglicheau D: Autophagy protects renal tubular cells against cyclosporine toxicity. Autophagy 2008, 4:783–791
32. Lieberthal W: Macroautophagy: a mechanism for mediating cell death or for promoting cell survival? Kidney Int 2009, 74:555–557
33. Hoyer-Hansen M, Jäättelä M: Connecting endoplasmic reticulum stress to autophagy by unfolded protein response and calcium. Cell Death Differ 2007, 14:1576–1582
34. Fung C, Lock R, Gao S, Salas E, Debnath J: Induction of autophagy during extracellular matrix detachment promotes cell survival. Mol Biol Cell 2008, 19:797–806
35. Kriz W, Le Hir M: Pathways to nephron loss starting from glomerular diseases - Insights from animal models. Kidney Int 2005, 67:404–419
36. Faulkner J, Szcykalski L, Springer F, Barnes J: Origin of interstitial fibroblasts in an accelerated model of angiotensin II-induced renal fibrosis. Am J Pathol 2005, 167:1193–1205
37. Duymelinck C, Dauwe S, De Greef K, Ysebaert D, Verpooten G, De Broe M: TIMP-1 gene expression and PAI-1 antigen after unilateral ureteral obstruction in the adult male rat. Kidney Int 2000, 58: 1186–1201
38. Kuusniemi A-M, Merenimes J, Lahdenkari A-T, Holmberg C, Salmela K, Karikoski R, Rapola J, Jalanko H: Glomerular sclerosis in kidneys with congenital nephrotic syndrome (NPHS1). Kidney Int 2006, 70:1423–1431
39. Fujigaki Y, Sun D, Fujimoto T, Yonemura K, Morioka T, Yaoita E, Hishida A: Cytokines and cell cycle regulation in the fibrous progression of crescent formation in antiglomerular basement membrane nephritis of WKY rats. Virchows Arch 2004, 439:35–45
40. Pozdzik A, Salmon I, Debelle F, Decaestecker C, Van den Branden C, Verbeelen D, Deschodt-Lanckman M, Vanherwghem J, Nortier J: Aristolochic acid induces proximal tubule apoptosis and epithelial to mesenchymal transformation. Kidney Int 2008, 73:595–607
41. Lin SL, Kisseleva T, Brenner D, Duffield J: Pericytes and perivascular fibroblasts are the primary source of collagen-producing cells in obstructive fibrosis of the kidney. Am J Pathol 2009, 173:1617–1627
42. Humphreys B, Lin SL, Kobayashi A, Hudosn T, Nowlin B, Bonventre J, Valerius M, McMahon A, Duffield J: Fate tracing reveals the pericyte and not epithelial origin of myofibroblasts in kidney fibrosis. Am J Pathol 2010, 176:85–97
43. Schnaper H, Jandeska S, Runyan C, Hubchak S, Basu R, Curley J, Smith R, Hayashida T: TGF-beta signal transduction in chronic kidney disease. Front Biosci 2009, 14:2448–2465 19273211
44. Hagedorn L, Floris J, Suter U, Sommer L: Autonomic neurogenesis and apoptosis are alternative fates of progenitor cell communities induced by TGFbeta. Dev Biol 2000, 228:57–72 11087626
45. Wu D, Bitzer M, Ju W, Mundel P, Bottinger E: TGF-beta concentration specifies differential signaling profiles of growth arrest/differentiation and apoptosis in podocytes. J Am Soc Nephrol 2005, 16:3211–3221